How Do Ultra-Low Frequency Waves Access the Inner Magnetosphere During Geomagnetic Storms?

I. Jonathan Rae[1] [ID], **Kyle R. Murphy[2]** [ID], **Clare E.J. Watt[3]** [ID], **Jasmine K. Sandhu[1]** [ID], **Marina Georgiou[1]** [ID], **Alex W. Degeling[4]** [ID], **Colin Forsyth[1]** [ID], **Sarah N. Bentley[3]** [ID], **Frances A. Staples[1]** [ID], and **Quanqi Shi[4]** [ID]

[1]Mullard Space Science Lab, UCL, Holmbury St Mary, UK, [2]Department of Astronomy, University of Maryland, College Park, MD, USA, [3]Department of Meteorology, University of Reading, Reading, UK, [4]Shandong Provincial Key Laboratory of Optical Astronomy and Solar-Terrestrial Environment, Institute of Space Sciences, Shandong University, Weihai, China

Abstract Wave-particle interactions play a key role in radiation belt dynamics. Traditionally, ultra-low frequency (ULF) wave-particle interaction is parameterized statistically by a small number of controlling factors for given solar wind driving conditions or geomagnetic activity levels. Here we investigate solar wind driving of ULF wave power and the role of the magnetosphere in screening that power from penetrating deep into the inner magnetosphere. We demonstrate that during enhanced ring current intensity, the Alfvén continuum plummets, allowing lower frequency waves to penetrate deeper into the magnetosphere than during quiet periods. With this penetration, ULF wave power is able to accumulate closer to the Earth than characterized by statistical models. During periods of enhanced solar wind driving such as coronal mass ejection driven storms, where ring current intensities maximize, the observed penetration provides a simple physics-based reason for why storm time ULF wave power is different compared to nonstorm time waves.

Plain Language Summary Geomagnetic storms are the most dynamic and unpredictable phenomena in near-Earth space. During geomagnetic storms, the Van Allen Radiation Belts can be significantly enhanced, via a number of physical processes. One of these processes is the action of large-scale ultra-low frequency waves, which are in large part directly related to the prevailing solar wind conditions. In this study, we show that the conditions and internal structuring in near-Earth space during a geomagnetic storm dictate how close to the Earth these large-scale waves can reach. Through a combination of ground-based and in situ measurements, we show how magnetic field strength and heavy ions control where these waves can access. We show that conditions both internal and external to near-Earth space must be taken into account to understand the behavior of waves, and therefore radiation belt particle dynamics, during geomagnetic storms.

1. Introduction

To provide a physically sound basis for models of energetic, relativistic electron dynamics (with energies >500 keV) in the radiation belts, the balance between acceleration, transport, and loss processes must be known. Electromagnetic waves across a large range of frequencies mediate the energy transfer processes in the plasma through a myriad of wave-particle interactions. This is especially true during geomagnetic storms, where the electrons in the radiation belt and the electromagnetic waves shaping their dynamics are at their most variable (Murphy et al., 2016; Watt et al., 2017).

Very low frequency (VLF) chorus waves play a fundamental role in radiation belt electron dynamics driving loss to the upper atmosphere (O'Brien et al., 2004) and acceleration within the heart of the outer radiation belt (Reeves et al., 2013). These waves are a critical process for modeling storm time dynamics of the outer radiation belt (Thorne et al., 2013). Electromagnetic ion cyclotron and VLF hiss waves are largely associated with rapid and slow loss from the radiation belts, respectively (Loto'aniu, Thorne, et al., 2006; Thorne et al., 2013). ULF waves transport and energize electrons via discrete resonances (e.g., Mann et al., 2013) and diffusive radial transport (e.g., Fälthammar, 1965).

Recent work demonstrated that both ULF and VLF waves are highly variable during storms and poorly characterized by empirical wave models (e.g., Ma et al., 2018; Murphy et al., 2016; Tu et al., 2013; Watt et al.,

2017). For instance, Tu et al. (2013) have shown that event-specific VLF chorus diffusion coefficients can be 2 orders of magnitude larger than to those derived from empirical models. Murphy et al. (2016) demonstrated that storm time ULF wave power is highly variable and can be several orders of magnitude larger than that predicted by empirical wave models.

It is not well understood why differences should exist between storm time and non–storm time waves. The basic concept of MHD wave propagation in the magnetosphere is that for a given wave frequency, its penetration is determined by the background magnetic field profile, the mass density, and azimuthal wavenumber (Lee, 1996; Figure 4). MHD waves will partially reflect, and the wave power will evanesce where the MHD wave mode reaches a turning point (i.e., the cutoff frequency exceeds the wave frequency). The fundamental mode eigenfrequency lies earthward of the turning point. Consequently, the global eigenfrequency configuration is indicative of how deeply ULF wave power of a given frequency and wavenumber can access the inner magnetosphere. Here we investigate a storm occurring during the Van Allen Probe era to determine why storm time ULF wave power may be so different than statistical norms.

2. 2013 St Patrick's Day Storm

2.1. General Overview

The 2013 St. Patrick's Day storm forms one of the radiation belt challenge events from the Quantitative Assessment of Radiation Belt Modeling focus group of the Geospace Environment Modeling program (http://bit.ly/28UnLpw) that has already been remarkably well studied in the literature (e.g., Albert et al., 2018; Engebretson et al., 2018; Ma et al., 2018). Figure S1 in the supporting information shows an overview of the solar wind and magnetospheric observations from 15 to 21 March 2013 inclusive and the overview of the event.

2.2. Background Alfvén Continuum

ULF waves generated at the magnetopause as a result of the interaction of the Earth's magnetosphere with the solar wind are reflected and refracted as they approach the inner magnetosphere by the Alfvén continuum (e.g., Mathie et al., 1999). The Alfvén continuum determines how deep fast mode waves with a specific frequency may propagate into the magnetosphere from the magnetopause. ULF waves generated at the magnetopause propagate radially inwards without generally losing energy. The Alfvén continuum determines the location at which the fast mode would enter the evanescent regime, and at which point the fast mode can couple to the Alfvén mode and drive toroidal-mode field line resonances (Samson et al., 1971).

It is difficult to determine the global Alfvén continuum from space-based measurements; however, this is routinely possible for the dayside hemisphere from ground-based magnetometer measurements (e.g., Waters et al., 1991). Cross-phase analysis can determine the fundamental resonant eigenfrequency between two magnetometer stations (Supporting Information S2), and we use the CARISMA (Canadian Array for Realtime Investigations of Magnetic Activity; Mann et al., 2008) array, using the technique documented by Sandhu, Yeoman, James, et al. (2018).

Figure 1 shows the results of this automated cross-phase analysis. Each panel displays the median field line eigenfrequency as a function of L-shell, separated into dawn sector (0600-1200 MLT, solid lines) and dusk sectors (1200-1800MLT, dashed lines) for each of the days of 15-21 March 2013 inclusive.

Field line eigenfrequencies are dependent upon the length of, and Alfvén velocity along, a given field line. During normal conditions, the eigenfrequency decreases monotonically with radial distance in regions inside and outside the plasmapause because the dominant magnetic field strength decays and field line lengths increase. Across the plasmapause, the plasma density drops sharply with radial distance, and the eigenfrequency will increase with radial distance over a short span of L (see Figure F1, Kale et al., 2007).

On 15 March 2013, the Alfvén eigenfrequency continuum displays the same behavior described above, with a small plasmapause reversal between L = 4.2 – 4.3 in the dusk sector. During 16 March 2013, the eigenfrequency profile is highly variable, at increased or similar frequencies across all L-shells in the dawn sector. In the dusk sector, eigenfrequencies decrease slightly at low-L and increase sharply at L~5, which may indicate the presence of a plasmaspheric plume.
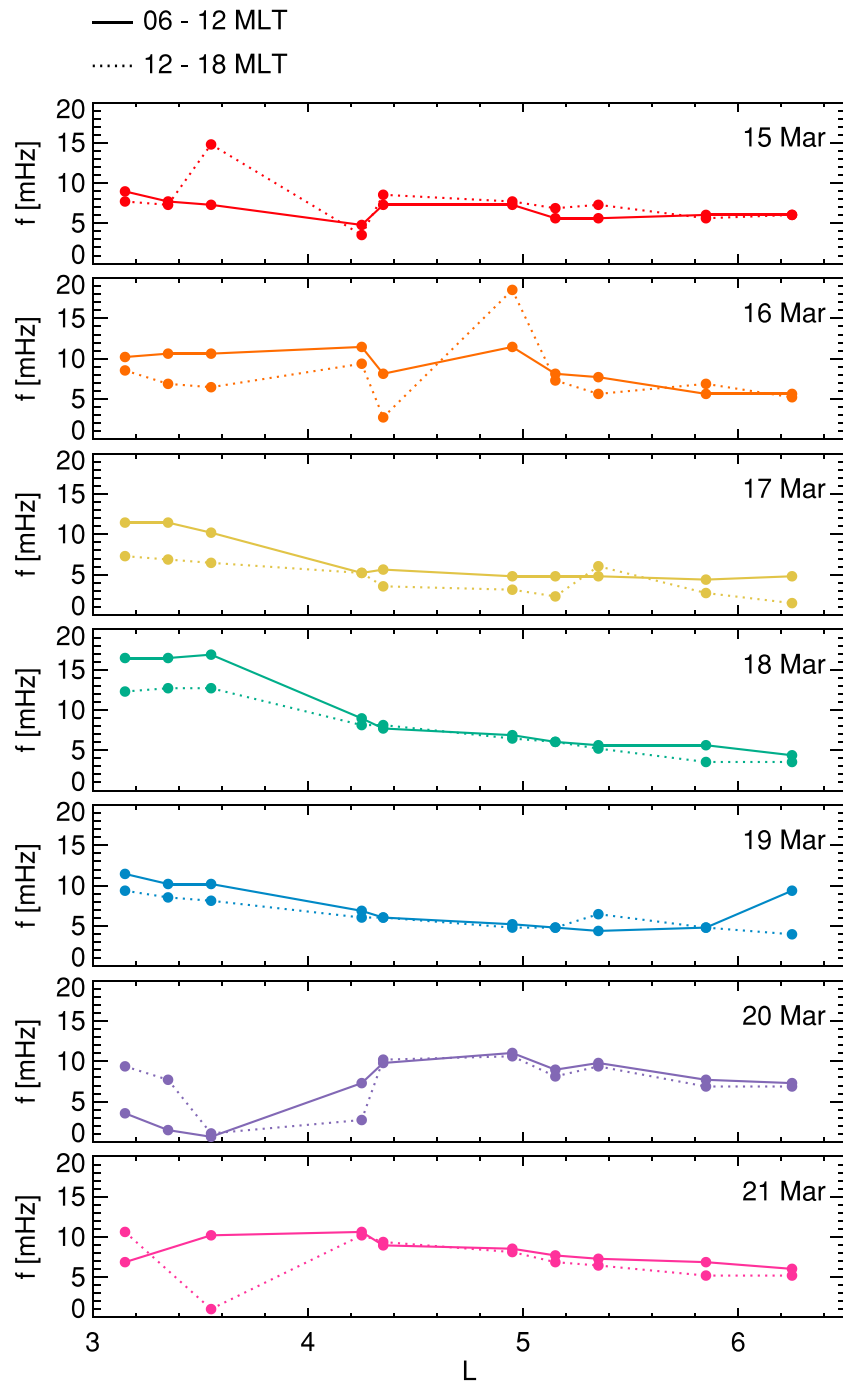
Figure 1. Eigenfrequency profiles from the Canadian Array for Realtime Investigations of Magnetic Activity (CARISMA) magnetometer array "Churchill Line" (see Supporting Information S2). Figure 1 contains the cross-phase results using the automated algorithm from Sandhu, Yeoman, James, et al. (2018) from measurements from station pairs shown in Supporting Information S2.

On 17 March 2013, however, there is little evidence of any increasing plasmapause gradient in the continuum across all L and the eigenfrequencies have reduced across all L-shells outside L = 3.4. There is some evidence of an MLT asymmetry: that dawn eigenfrequencies are higher than those at dusk. This reduction in the Alfvén continuum is concurrent with the arrival of the coronal mass ejection (CME) and the initiation of this geomagnetic storm around 0500 UT.
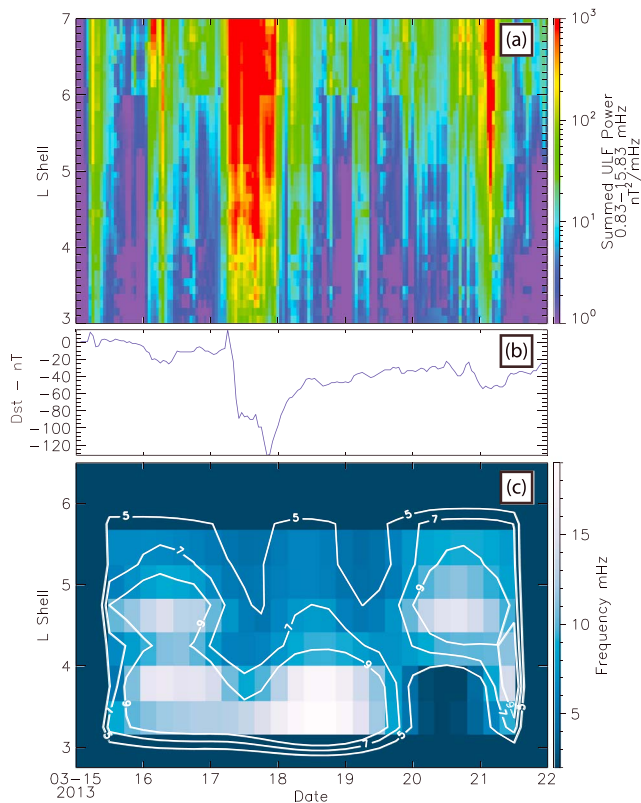
Figure 2. (a) Summed ultra-low frequency wave power from the IMAGE and Canadian Array for Realtime Investigations of Magnetic Activity (CARISMA) magnetometer chains for the 15-22 March 2013 storm over the dayside magnetosphere (06-18 MLT) interpolated onto a 2-D grid with 1 hr resolution and 0.1-L step (original data in Supporting Information S2). (bottom) a 2-D interpolation with 6 hr in time and 0.25-L spatial scales of the Alfvén continuum shown in Figure 1.

On 18 March 2013, there are still some dawn-dusk differences in eigenfrequency profiles inside of L = 4.2, whereby dawn frequencies are up to 50% higher than their dusk counterparts. All eigenfrequencies inside of L~5 are also higher than their counterparts on the previous day. Both increases in eigenfrequencies and asymmetries in the plasmaspheric density are consistent with the presence of the remnants of a plasmaspheric density plume of the previous day (e.g., Borovsky & Denton, 2008).

On 19 March 2013, the eigenfrequency profiles return to similar values as 17 March 2013, and the differences between the dawn and dusk asymmetries have reduced. Toward the end of the period examined, on 20 and 21 March 2013, significant MLT and L-shell variations are found. The eigenfrequency profiles are very different in each MLT sector, and the eigenfrequency values at around L=5 are much larger than they were on 19 March 2013. These major changes are coincident with the arrival of the secondary CME (see previous section) at around 1200 on 20 March 2013. We discuss these changes in the eigenfrequency profile in terms of plasma density evolution through the two consecutive geomagnetic storms.

2.3. Storm time ULF wave power

We take the vector summed power from the CARISMA (Mann et al., 2008) and IMAGE (Lühr, 1994) magnetometer networks throughout the storm across 51 magnetometers in the same manner as Murphy et al. (2015, 2016) and Mann et al. (2016) and limit our analysis to the dayside hemisphere only and compare this with Figure 1. We limit the analysis to the dayside such that the powers are not influenced by substorm activity (Murphy et al., 2011; Rae et al., 2011).

We use 51 magnetometers to calculate the summed ULF power between 0.83 and 15.83 MHz at 1-hr resolution throughout the storm period and interpolated onto a uniform 2-D grid (original data, Supporting Information S3).

Figure 2a shows the results of this ground-based analysis of summed ULF wave power as a function of L and time from 15 to 22 March 2013. Clear from Figure 2a is that the ULF wave activity is highly time-dependent during the period of interest. The ULF wave power across the storm varies both in strength and in penetration depth into the magnetosphere and across multiple frequencies (see Supporting Information S4).

There are also interesting ULF wave signatures at other times that can be associated with other solar wind drivers. Two enhancements in ULF wave power across all L are seen early on 15 March 2013 and the morning of 16 March 2013. Using the statistical results of Bentley et al. (2018) as an aid, the ULF wave power enhancements on the morning of 15 March 2013 are likely related to the large change in plasma density and negative interplanetary magnetic field (IMF) B_z seen in the solar wind. A similar negative IMF B_z deflection accompanied by a smaller change in plasma density is also seen on the morning of 16 March 2013. Prior to the CME arrival (17 March 2013), the ULF wave activity was quiet and significant ULF wave power (10 nT^2/MHz) was not seen any further inside the magnetosphere than L~6. However, on arrival of the CME, the ULF waves are enhanced across all L-shells, the power increasing to >10^3 nT^2/MHz at high L, and reaching $10^2 nT^2$/MHz at L=3. The increase in ULF wave activity at high L is likely associated with the significant increase in solar wind velocity and negative IMF B_z that accompany the start of the CME, but what is most interesting is just how far inside the magnetosphere the increase in ULF wave power is seen.

In the ensuing recovery phase on 18 March 2013, the ULF wave power reduces in strength across all locations. Interestingly, the wave amplitude at high L is fairly constant throughout 18 March and into the morning of 19 March 2013. However, the wave activity increases abruptly at lower L in the early hours of 19 March 2013 before decreasing again to a background level a few hours later.

Finally, on the morning of the 21 March 2013, ULF wave power is once again enhanced, reaching 103 nT^2/MHz at high L, and >101 nT^2/MHz at L=3, presumably due to the arrival of the second CME with its increase in solar wind velocity and subsequent ULF energization. We discuss the role of external driving and internal background Alfvén continuum in this energization below.

Figure 2c shows a 2-D interpolation of the results shown in Figure 1 of the Alfvén continuum as a function of L-shell and time where color indicates frequency. A similar type of interpolation has been performed as in the top panel, with a 6 hr time scale, and 0.5-L spatial scale. Overplotted in Figure 2c are isocontours of specific frequencies (5, 7, and 9 MHz) to highlight the variability of the location of a particular eigenfrequency over the course of the interval.

Figure 2c shows that there is significant structuring of the Alfvén continuum as a function of L and time. Specifically, if we consider the propagation of ULF waves inward through the magnetosphere, then the continuum structure prior to the storm (i.e., on 15 and 16 March 2013) would enable ULF wave energy at high frequencies (>10 MHz) to access the inner magnetosphere, but frequencies lower than that would be reflected and refracted or evanesce. However, once the storm main phase has commenced, the eigenfrequency profile reduces dramatically, such that wave frequencies of 5 MHz could propagate into the inner magnetosphere without hindrance. The 9 MHz contour moves in to L<3.5 after the storm modifies the magnetosphere, as compared to the period prior to the storm where the 9 MHz contour exists at L>5. Figure S4 shows ULF wave power at these specific frequencies of 5, ~7, and ~9 MHz and demonstrates that the ULF wave power at given frequencies does indeed penetrate to lower-L when the eigenfrequency continuum is suppressed.

As the storm moves into the recovery phase, the ULF wave power in Figure 2a wanes at higher L-shells, at the same time as the Alfvén continuum relaxes, such that 5-MHz contours are now around L=6. On 19 March 2013, the Alfvén continuum again reduces to a storm-like level, and we observe another ULF wave penetration event (Figure 2, top). Finally, Figure 2c shows that toward the end of the interval, at the same time as the second, smaller storm, the pattern of the eigenfrequency continuum is reversed such that low frequencies are observed at low L and vice versa. We conclude that either the plasmapause is around L~4 and the eigenfrequency continuum returns to a more typical profile (cf., Figure 1, Kale et al., 2007) or that there may be a complicated Alfvén continuum due to the recovery phase of one storm coinciding with another.

3. Discussion and Conclusions

ULF waves are a key component of any storm time study of relativistic electron dynamics, whether they are responsible for direct energization (Claudepierre et al., 2013), transport (Mann et al., 2016; Ozeke et al., 2018), or losses (e.g., Rae et al., 2018). Here we investigate the role of ULF waves during a geomagnetically active period, with the critical addition of using the eigenfrequency continuum to monitor the changes in the internal environment of the magnetosphere, as seen by the ULF waves.

It is now established that the main source of global-scale ULF wave power is the solar wind. Global-scale ULF waves have low azimuthal wavenumbers, m, the value of which describes the number of wavelengths around the Earth at a given radial distance. Solar wind speed (Mathie & Mann, 2001; Murphy et al., 2011; Rae et al., 2012) and dynamic pressure (Kepko et al., 2002; Sibeck et al., 1989) have both been studied as controlling factors. However, the interdependence of solar wind parameters can often mask the underlying factors that result in enhanced ULF wave power, necessitating a systematic statistical study. Recently, the relative contributions of solar wind drivers of ULF wave power have been quantified by Bentley et al. (2018). In this work, Bentley et al. (2018) found that solar wind speed was the dominant driver, followed by the southward component of IMF B_z and, in contrast to previous work, the variance in number density, as opposed to the derived dynamic pressure. Statistically, as solar wind driving enhances, ULF wave power increases monotonically at all radial distances in the inner magnetosphere (e.g., Georgiou et al., 2018; Mathie et al., 1999; Rae et al., 2012). However, none of these previous statistical studies take into account the time history of the solar wind, including the temporal behavior of CMEs, corotating interaction regions, or other solar wind transients. Hence, the time-dependent nature of the solar wind may be a critical missing factor in empirical models of solar wind-driven ULF wave activity.

Equally, the internal plasma conditions of the magnetosphere are typically not considered in parameterized models of ULF wave power. Such models often use a geomagnetic index as a proxy for the external solar

wind driving and internal magnetospheric dynamics (e.g., the Kp model of Ozeke et al., 2012, 2014). Physically, ULF wave activity in the magnetosphere is dictated by the background magnetic field strength and the number density and composition of the cold plasma. It is these parameters that control the Alfvén eigenfrequency profile and hence the accessibility of ULF wave power into a given magnetospheric location.

Figure 1 shows the variation of the Alfvén continuum with L-shell, frequency, and time throughout the 2013 St. Patrick's Day storm. During the storm main phase, the Alfvén continuum is suppressed at the vast majority of L-shells, other than around L=3.4 where there is some evidence of a newly formed or refilling plasmapause. The consequence of this is that prior to the storm, only frequencies greater than 12 MHz could access the inner magnetosphere without evanescently decaying. During the main phase of the storm, suddenly any frequencies greater than 5 MHz can now penetrate into the inner magnetosphere as deep as L=3.4.

During this storm, the ULF wave power (Figure 2, top) is highly dynamic, varying by 3 orders of magnitude. Storm time ULF wave power has been shown to be significantly variable during the main phase of the storm (e.g., Loto'aniu, Mann, et al., 2006; Murphy et al., 2016). During one of the largest geomagnetic storms in recent history, the "Halloween storm" of 2003, Loto'aniu, Mann, et al. (2006) found that ULF wave power varied by 4 orders of magnitude. Interestingly, these authors also found that ULF wave power was most enhanced during the two storm main phases. More specifically, the largest ULF wave power during the Halloween storm occurred during the three periods of increasingly negative Dst index.

During periods where the eigenfrequencies are lower, ULF wave power reaches deeper into the magnetosphere (Figure 2). ULF wave power inside the magnetosphere has a power law like power spectrum (Bentley et al., 2018; Rae et al., 2012). Hence, when lower frequencies can access lower L-shells, the summed ULF wave power is generally higher. When the Alfvén profile recovers between 19 and 20 March 2013, ULF wave power is screened from the inner magnetosphere. However, when the second geomagnetic storm occurs on the 20 March 2013, ULF wave power again accesses the inner magnetosphere. By inspection of Figures 1 and 2, it is clear that the eigenfrequency variations are complex, but this may result in plasmaspheric plumes significantly complicating the simple ULF wave dynamics that are described in the current literature. Essentially, when there are both radial and azimuthal gradients in the Alfvén continuum, there is a frequency-dependent accumulation and penetration of ULF wave power through, and indeed within, the plume (cf., Figure 3a; Degeling et al., 2018), which will complicate the magnetospheric location of ULF wave powers.

The natural eigenfrequency of geomagnetic field lines is determined by its magnetic field profile and the mass density along the field line. During geomagnetic storms, it is usually thought that heavy ion outflow increases the mass density sufficiently to lower the Alfvén continuum (e.g., Engwall et al., 2009; Kale et al., 2009; Kronberg et al., 2014; Loto'aniu, Mann, et al., 2006; Yau et al., 1988). Certainly heavy ions must play a role. However, Sandhu, Yeoman, and Rae (2018) constructed a statistical model of the average mass densities as a function of Dst index. Sandhu, Yeoman, and Rae (2018) found that although the average ion mass did increase significantly with increasingly negative Dst index, the electron densities in the inner magnetosphere reduced.

Hence, on average, lower Dst index values reduce the plasma mass density, rather than increasing it as previously thought. Sandhu, Yeoman, and Rae (2018) concluded that the changes in the magnetic field drove the changes in eigenfrequency; during sudden increases in dayside compression, the geomagnetic field strength in the outer magnetosphere increases across the dayside. It is important to remember that when using a proxy such as Dst index, two very different intervals are averaged, decreasing Dst during the main phase and increasing Dst during the recovery phase even though both phases pass through the same values of Dst. However, Sandhu, Yeoman, and Rae (2018) model provides useful context for interpreting our results. We now consider the role of the ring current itself in reducing the Alfvén continuum in the inner magnetosphere. Commonly, the "Dst effect" (Kim & Chan, 1997) is specifically limited to the effect of ring current enhancement encouraging electron loss. Here we suggest that the strengthening ring current significantly changes the Alfvén continuum during key periods of the storm.

Relationships between ring current intensity and ULF wave power have been discussed previously (e.g., Mann et al., 2012; Murphy et al., 2014), suggesting a causal link between ring current ions and the generation of storm time high-m waves that could play additional roles in energization (e.g., Ozeke & Mann, 2008)
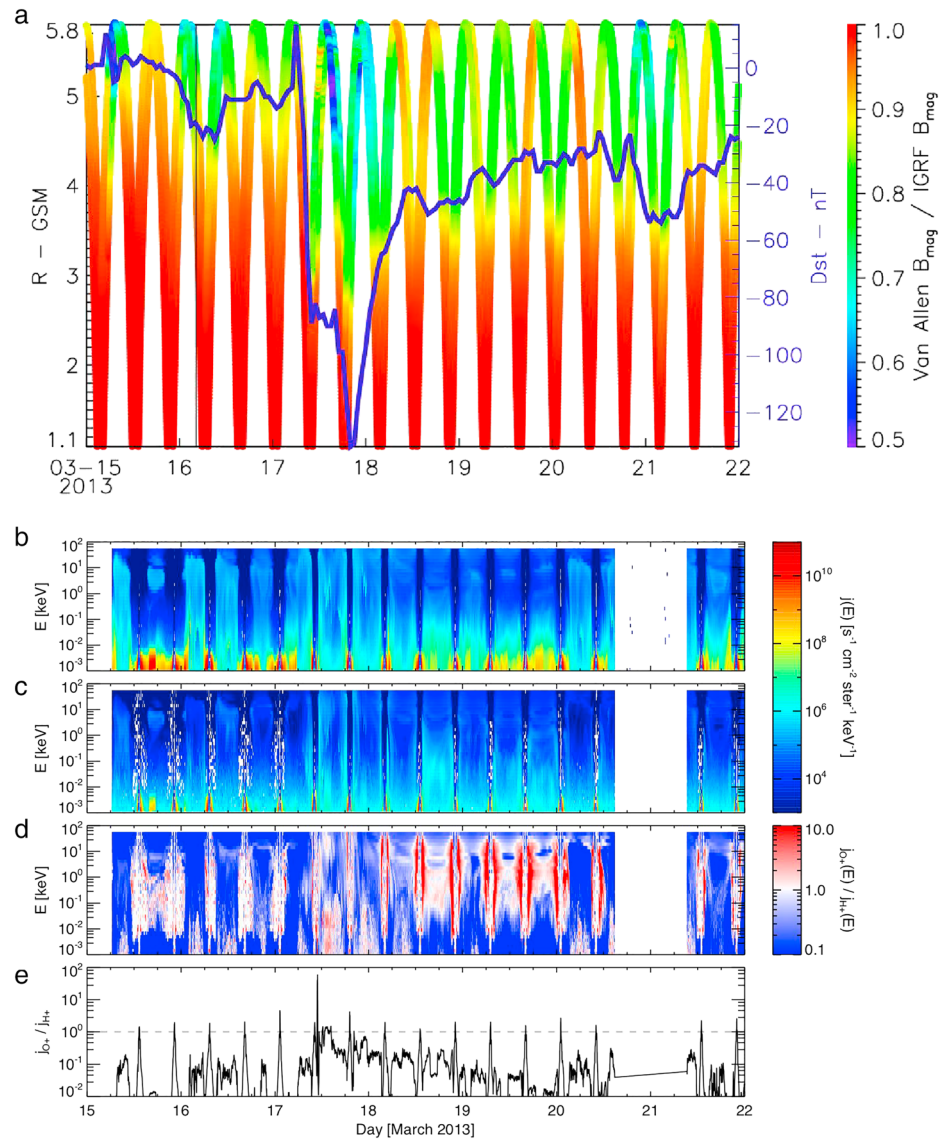
AGU
100
ADVANCING EARTH
AND SPACE SCIENCE

Geophysical Research Letters

10.1029/2019GL082395

Figure 3. (a) Comparison between observed field magnitude from Van Allen Probes A and B and the International Geomagnetic Reference Field model. Figure 3a shows the ratio of observed magnitude to International Geomagnetic Reference Field magnitude as a function of radial distance and time. Overplotted on the right axis is the Dst index. (b-e). Helium Oxygen Proton Electron (HOPE) observations of omnidirectional energy flux for H+ ions, jH+(E), and O+ ions, jO+(E), averaged at 5-min resolution from 15 to 22 March 2015. Figures 3b and 3c indicate energy spectrograms of jH+(E) and jO+(E), respectively. Figure 3d indicates energy spectrogram showing the ratio of jO+(E) to jH+(E). Figure 3e indicates the ratio of jO+(E) to jH+(E) summed over all energies shown in Figure 3d.

and loss (e.g., Rae et al., 2018). Clearly, it is the interplay between magnetic field and plasma mass densities that is key during the dynamic period in main phase of the storm. Figures 2c and 3e show that the eigenfrequencies are suppressed during this storm main phase.

In order to reduce the Alfvén continuum across a wide range of L-shells, the magnetic field strength must reduce, or the mass density must increase, or a combination of both. Figure 3a demonstrates the effect of the ring current in reducing the local magnetic field strength at the Van Allen Probes A and B throughout the storm, by displaying the ratio between the magnetic field strength observed by Van Allen Probes (Kletzing et al., 2013) relative to the International Geomagnetic Reference Field. Note that there is a clear reduction in the ratio away from 1.0 in the same manner as Shen et al. (2014) discussed that is mirrored by the negative enhancement in the Dst index. This implies that the expected magnetic field as measured

by the Van Allen Probes is significantly suppressed during the storm main phase and in response to the evolving ring current.

There are a number of factors at play here, however. Field line eigenfrequencies are influenced by the magnetic field strength and by plasma mass density along the field. In this paper, we discuss how the inner magnetosphere could respond differently to geomagnetic storms than the outer magnetosphere. Ion outflow during geomagnetic storms (e.g., Yau et al., 1988) would certainly influence the plasma mass density at all locations during the main phase of the storm. However, there is also a secondary effect, which is that there is also enhanced helium and oxygen ring current ions in the inner magnetosphere (e.g., Sandhu, Rae, et al., 2018). The enhanced ring current (and its contribution to mass densities) will increase the heavy ion content in the inner magnetosphere, while also reducing the local magnetic field strength at ring current radial distances (Kim & Chan, 1997; Kronberg et al., 2014). Regardless of which effect is dominant, these additive effects lead to a net decrease in the Alfvén continuum, allowing deep penetration of ULF wave power into the inner magnetosphere during periods of increase ring current intensity. It must be stressed that the amplitude of this ULF wave accessibility is dependent upon the solar wind driver and, while penetration can occur during ring current enhancements, large amplitude wave power at low-L will occur during periods of enhanced solar wind driving and ring current intensities (e.g., Loto'aniu, Mann, et al., 2006). The plasmapause role on Pc5 penetration has been reported before by Hartinger et al. (2010). Here we discuss that multiple storm time factors of plasma composition and density, global magnetic field configuration, and the suppression of the inner magnetospheric field by the ring current can depress the Alfvén continuum.

Figures 3b–3e show ion data from the Van Allen Probes HOPE (Helium Oxygen Proton Electron) instruments (Funsten et al., 2013; Spence et al., 2013) during the storm. Figures 3b–3e show (b) H+, (c) O+ energy fluxes as a function of energy and time, and (d) the ratio between these fluxes. Figure 3c shows the increase in both low energy oxygen (<100 eV) on 17 March 2013 at ~12 UT, and the delayed increase of higher energy oxygen (100eV-100keV) later in the geomagnetic storm from 12 UT on 18 March 2013, and with a slow decay lasting ~1-2 days. This two-step heavy ion increase is consistent with the sharp increase in ion outflow at the start of the geomagnetic storm (e.g., Gkioulidou et al., 2019; Kronberg et al., 2014) and the longer-term penetration of heavy ions convected into the inner magnetosphere from substorms (e.g., Sandhu, Rae, et al., 2018). Figure 3d shows the ratio of oxygen to hydrogen as a function of energy, and Figure 3e summed over energy to demonstrate intervals where the heavy ion content of the ring current should be considered to be significant; the dashed horizontal line indicates unity. On 17 March, the increase in low-energy oxygen and the decrease in low-energy hydrogen lead to a large increase in the ratio. The hydrogen content of the ring current recovers over the course of the 18 March 2013, and there is an additional higher energy oxygen content, which maintains an elevated ratio as seen in Figure 3e. The additive effect of reduced magnetic field and two-step heavy ion content leads to a suppressed Alfvén continuum that is highly variable throughout the entire storm time period, enabling MHz frequencies to penetrate the inner magnetosphere as a consequence. We conclude that solar wind driving as well as current internal conditions must both be considered for realistic storm time ULF wave conditions in the inner magnetosphere.

It is interesting to note that the lowering of the continuum and penetration of ULF wave power is closely coincident with the time and location of rapid enhancement in MeV electron fluxes (Figure S1), as both ULF wave power and enhancements occur around L=3-3.5. Such penetration may also explain slot region filling during very large storms, where both ULF wave powers and ring current intensities are largest (Ozeke et al., 2018). What role this ULF wave power plays in shaping the radiation belt enhancement remains to be seen, but what is clear is that ULF wave powers must be taken into account during radiation belt modeling of such enhancements.

One of the primary challenges of the Quantitative Assessment of Radiation Belt Morphology (QARBM) Geospace Environment Modeling challenge is to assess the validity of diffusion coefficients during specific geomagnetic storms. Since the accessibility of ULF wave power is strongly dependent upon internal geomagnetic conditions, we conclude that the radial dependence of ULF wave diffusion coefficients will vary significantly during geomagnetic storms not only on external driving but also critically on internal factors that have not yet been fully considered.

References

Albert, J. M., Selesnick, R. S., Morley, S. K., Henderson, M. G., & Kellerman, A. C. (2018). Calculation of last closed drift shells for the 2013 GEM radiation belt challenge events. *Journal of Geophysical Research: Space Physics*, 123, 9597–9611. https://doi.org/10.1029/2018JA025991

Bentley, S. N., Watt, C. E. J., Owens, M. J., & Rae, I. J. (2018). ULF wave activity in the magnetosphere: Resolving solar wind interdependencies to identify driving mechanisms. *Journal of Geophysical Research: Space Physics*, 123, 2745–2771. https://doi.org/10.1002/2017ja024740

Borovsky, J. E., & Denton, M. H. (2008). A statistical look at plasmaspheric drainage plumes. *Journal of Geophysical Research*, 113, A09221. https://doi.org/10.1029/2007JA012994

Claudepierre, S. G., Mann, I. R., Takahashi, K., Fennell, J. F., Hudson, M. K., Blake, J. B., et al. (2013). Van Allen Probes observation of localized drift resonance between poloidal mode ultra-low frequency waves and 60 keV electrons. *Geophysical Research Letters*, 40, 4491–4497. https://doi.org/10.1002/grl.50901

Degeling, A. W., Rae, I. J., Watt, C. E. J., Shi, Q. Q., Rankin, R., & Zong, Q. G. (2018). Control of ULF wave accessibility to the inner magnetosphere by the convection of plasma density. *Journal of Geophysical Research: Space Physics*, 123, 1086–1099. https://doi.org/10.1002/2017JA024874

Engebretson, M. J., Posch, J. L., Braun, D. J., Li, W., Ma, Q., Kellerman, A. C., et al. (2018). EMIC wave events during the four GEM QARBM challenge intervals. *Journal of Geophysical Research: Space Physics*, 123, 6394–6423. https://doi.org/10.1029/2018JA025505

Engwall, E., Eriksson, A. I., Cully, C. M., André, M., Torbert, R., & Vaith, H. (2009). Earth's ionospheric outflow dominated by hidden cold plasma. *Nature Geoscience*, 2(1), 24–27. https://doi.org/10.1038/NGEO387

Fälthammar, C.-G. (1965). Effects of time-dependent electric fields on geomagnetically trapped radiation. *Journal of Geophysical Research*, 70(11), 2503–2516. https://doi.org/10.1029/JZ070i011p02503

Funsten, H. O., Skoug, R. M., Guthrie, A. A., MacDonald, E. A., Baldonado, J. R., Harper, R. H., et al. (2013). Helium, Oxygen, Proton, and Electron (HOPE) mass spectrometer for the Radiation Belt Storm Probes mission. *Space Science Reviews*, 179(1-4), 423–484. https://doi.org/10.1007/s11214-013-9968-7

Georgiou, M., Daglis, I. A., Rae, I. J., Zesta, E., Sibeck, D. G., Mann, I. R., et al. (2018). Ultra-low frequency waves as an intermediary for solar wind energy input into the radiation belts. *Journal of Geophysical Research: Space Physics*, 123, 10,090–10,108. https://doi.org/10.1029/2018JA025355

Gkioulidou, M., Ohtani, S., Ukhorskiy, A. Y., Mitchell, D. G., Takahashi, K., Spence, H. E., et al. (2019). Low-energy (<keV) O+ ion outflow directly into the inner magnetosphere: Van Allen Probes observations. *Journal of Geophysical Research: Space Physics*, 124, 405–419. https://doi.org/10.1029/2018JA025862

Hartinger, M., Moldwin, M. B., Angelopoulos, V., Takahashi, K., Singer, H. J., Anderson, R. R., et al. (2010). Pc5 wave power in the quiet-time plasmasphere and trough: CRRES observations. *Geophysical Research Letters*, 37, L07107. https://doi.org/10.1029/2010GL042475

Kale, Z. C., Mann, I. R., Waters, C. L., Goldstein, J., Menk, F. W., & Ozeke, L. G. (2007). Ground magnetometer observation of a cross-phase reversal at a steep plasmapause. *Journal of Geophysical Research*, 112, A10222. https://doi.org/10.1029/2007JA012367

Kale, Z. C., Mann, I. R., Waters, C. L., Vellante, M., Zhang, T. L., & Honary, F. (2009). Plasmaspheric dynamics resulting from the Hallowe'en 2003 geomagnetic storms. *Journal of Geophysical Research*, 114, A08204. https://doi.org/10.1029/2009JA014194

Kepko, L., Spence, H. E., & Singer, H. J. (2002). ULF waves in the solar wind as direct drivers of magnetospheric pulsations. *Geophysical Research Letters*, 29(8), 1197. https://doi.org/10.1029/2001GL014405

Kim, H.-J., & Chan, A. A. (1997). Fully adiabatic changes in storm time relativistic electron fluxes. *Journal of Geophysical Research*, 102(A10), 22,107–22,116. https://doi.org/10.1029/97JA01814

Kletzing, C. A., Kurth, W. S., Acuna, M., MacDowall, R. J., Torbert, R. B., Averkamp, T., et al. (2013). The Electric and Magnetic Field Instrument Suite and Integrated Science (EMFISIS) on RBSP. *Space Science Review*, 179(1-4), 127–181. https://doi.org/10.1007/s11214-013-9993-6

Kronberg, E. A., Ashour-Abdalla, M., Dandouras, I., Delcourt, D. C., Grigorenko, E. E., Kistler, L. M., et al. (2014). Circulation of heavy ions and their dynamical effects in the magnetosphere: Recent observations and models. *Space Science Reviews*, 184(1-4), 173–235. https://doi.org/10.1007/s11214-014-0104-0

Lee, D.-H. (1996). Dynamics of MHD wave propagation in the low-latitude magnetosphere. *Journal of Geophysical Research*, 101(A7), 15,371–15,386. https://doi.org/10.1029/96JA00608

Loto'aniu, T. M., Mann, I. R., Ozeke, L. G., Chan, A. A., Dent, Z. C., & Milling, D. K. (2006). Radial diffusion of relativistic electrons into the radiation belt slot region during the 2003 Halloween geomagnetic storms. *Journal of Geophysical Research*, 111, A04218. https://doi.org/10.1029/2005JA011355

Loto'aniu, T. M., Thorne, R. M., Fraser, B. J., & Summers, D. (2006). Estimating relativistic electron pitch angle scattering rates using properties of the electromagnetic ion cyclotron wave spectrum. *Journal of Geophysical Research*, 111, A04220. https://doi.org/10.1029/2005JA011452

Lühr, H. (1994). The IMAGE magnetometer network, STEP International (Vol. 4, pp. 4–6). USSCO.

Ma, Q., Li, W., Bortnik, J., Thorne, R. M., Chu, X., Ozeke, L. G., et al. (2018). Quantitative evaluation of radial diffusion and local acceleration processes during GEM challenge events. *Journal of Geophysical Research: Space Physics*, 123, 1938–1952. https://doi.org/10.1002/2017JA025114

Mann, I. R., Lee, E. A., Claudepierre, S. G., Fennell, J. F., Degeling, A., Rae, I. J., et al. (2013). Discovery of the action of a geophysical synchrotron in the Earth's Van Allen radiation belts. *Nature Communications*, 4(1). https://doi.org/10.1038/ncomms3795

Mann, I. R., Milling, D. K., Rae, I. J., Ozeke, L. G., Kale, A., Kale, Z. C., et al. (2008). The upgraded CARISMA magnetometer array in the THEMIS era. *Space Science Reviews*, 141(1-4), 413–451. https://doi.org/10.1007/s11214-008-9457-6

Mann, I. R., Murphy, K. R., Ozeke, L. G., Rae, I. J., Milling, D. K., Kale, A., & Honary, F. (2012). The role of ultralow frequency waves in radiation belt dynamics. In D. Summers, I. R. Mann, D. N. Baker, & M. Schultz (Eds.), *Dynamics of the Earth's Radiation Belts and Inner Magnetosphere* (pp. 69–91). Washington, DC: American Geophysical Union. https://doi.org/10.1029/2012GM001349

Mann, I. R., Ozeke, L. G., Murphy, K. R., Claudepierre, S. G., Turner, D. L., Baker, D. N., et al. (2016). Explaining the dynamics of the ultra-relativistic third Van Allen radiation belt. *Nature Physics*, 12(10), 978–983. https://doi.org/10.1038/nphys3799

Mathie, R. A., & Mann, I. R. (2001). On the solar wind control of Pc5 ULF pulsation power at mid-latitudes: Implications for MeV electron acceleration in the outer radiation belt. *Journal of Geophysical Research*, 106(A12), 29,783–29,796. https://doi.org/10.1029/2001JA000002

Mathie, R. A., Menk, F. W., Mann, I. R., & Orr, D. (1999). Discrete field line resonances and the Alfvén continuum in the outer magnetosphere. *Geophysical Research Letters*, *26*(6), 659–662. https://doi.org/10.1029/1999GL900104

Murphy, K. R., Mann, I. R., & Ozeke, L. G. (2014). A ULF wave driver of ring current energization. *Geophysical Research Letters*, *41*, 6595–6602. https://doi.org/10.1002/2014GL061253

Murphy, K. R., Mann, I. R., Rae, I. J., Sibeck, D. G., & Watt, C. E. J. (2016). Accurately characterizing the importance of wave-particle interactions in radiation belt dynamics: The pitfalls of statistical wave representations. *Journal of Geophysical Research: Space Physics*, *121*, 7895–7899. https://doi.org/10.1002/2016JA022618

Murphy, K. R., Mann, I. R., & Sibeck, D. G. (2015). On the dependence of storm time ULF wave power on magnetopause location: Impacts for ULF wave radial diffusion. *Geophysical Research Letters*, *42*, 9676–9684. https://doi.org/10.1002/2015GL066592

Murphy, K. R., Rae, I. J., Mann, I. R., & Milling, D. K. (2011). On the nature of ULF wave power during nightside auroral activations and substorms: 1. Spatial distribution. *Journal of Geophysical Research*, *116*, A00I21. https://doi.org/10.1029/2010JA015757

O'Brien, T. P., Looper, M. D., & Blake, J. B. (2004). Quantification of relativistic electron microburst losses during the GEM storms. *Geophysical Research Letters*, *31*, L04802. https://doi.org/10.1029/2003GL018621

Ozeke, L. G., & Mann, I. R. (2008). Energization of radiation belt electrons by ring current ion driven ULF waves. *Journal of Geophysical Research*, *113*, A02201. https://doi.org/10.1029/2007JA012468

Ozeke, L. G., Mann, I. R., Murphy, K. R., Degeling, A. W., Claudepierre, S. G., & Spence, H. E. (2018). Explaining the apparent impenetrable barrier to ultra-relativistic electrons in the outer Van Allen belt. *Nature Communications*, *9*(1), 1844. https://doi.org/10.1038/s41467-018-04162-3

Ozeke, L. G., Mann, I. R., Murphy, K. R., Jonathan Rae, I., & Milling, D. K. (2014). Analytic expressions for ULF wave radiation belt radial diffusion coefficients. *Journal of Geophysical Research: Space Physics*, *119*, 1587–1605. https://doi.org/10.1002/2013JA019204

Ozeke, L. G., Mann, I. R., Murphy, K. R., Rae, I. J., Milling, D. K., Elkington, S. R., et al. (2012). ULF wave derived radiation belt radial diffusion coefficients. *Journal of Geophysical Research*, *117*, A04222. https://doi.org/10.1029/2011JA017463

Rae, I. J., Mann, I. R., Murphy, K. R., Ozeke, L. G., Milling, D. K., Chan, A. A., et al. (2012). Ground-based magnetometer determination of in situ Pc4-5 ULF electric field wave spectra as a function of solar wind speed. *Journal of Geophysical Research*, *117*, A04221. https://doi.org/10.1029/2011JA017335

Rae, I. J., Murphy, K. R., Watt, C. E. J., Halford, A. J., Mann, I. R., Ozeke, L. G., et al. (2018). The role of localised compressional ultra-low frequency waves in energetic electron precipitation. *Journal of Geophysical Research: Space Physics*, *123*, 1900–1914. https://doi.org/10.1002/2017ja024674

Rae, I. J., Murphy, K. R., Watt, C. E. J., & Mann, I. R. (2011). On the nature of ULF wave power during nightside auroral activations and substorms: 2. Temporal evolution. *Journal of Geophysical Research*, *116*, A00I22. https://doi.org/10.1029/2010JA015762

Reeves, G. D., Spence, H. E., Henderson, M. G., Friedel, R. H. W., Funsten, H. O., Baker, D. N., et al. (2013). Electron acceleration in the heart of the Van Allen radiation belts. *Science*, *341*(6149), 991–994. https://doi.org/10.1126/science.1237743

Samson, J. C., Jacobs, J. A., & Rostoker, G. (1971). Latitude dependent characteristics of long-period geomagnetic pulsations. *Journal of Geophysical Research*, *76*(16), 3675–3683. https://doi.org/10.1029/JA076i016p03675

Sandhu, J. K., Rae, I. J., Freeman, M. P., Forsyth, C., Gkioulidou, M., Reeves, G. D., et al. (2018). Energization of the ring current by substorms. *Journal of Geophysical Research: Space Physics*, *123*, 8131–8148. https://doi.org/10.1029/2018JA025766

Sandhu, J. K., Yeoman, T. K., James, M. K., Rae, I. J., & Fear, R. C. (2018). Variations of high-latitude geomagnetic pulsation frequencies: A comparison of time-of-flight estimates and IMAGE magnetometer observations. *Journal of Geophysical Research: Space Physics*, *123*, 567–586. https://doi.org/10.1002/2017JA024434

Sandhu, J. K., Yeoman, T. K., & Rae, I. J. (2018). Variations of field line eigenfrequencies with ring current intensity. *Journal of Geophysical Research: Space Physics*, *123*, 9325–9339. https://doi.org/10.1029/2018JA025751

Shen, C., Yang, Y. Y., Rong, Z. J., Li, X., Dunlop, M., Carr, C. M., et al. (2014). Direct calculation of the ring current distribution and magnetic structure seen by Cluster during geomagnetic storms. *Journal of Geophysical Research: Space Physics*, *119*, 2458–2465. https://doi.org/10.1002/2013JA019460

Sibeck, D. G., Baumjohann, W., Elphic, R. C., Fairfield, D. H., & Fennell, J. F. (1989). The magnetospheric response to 8-minute period strong-amplitude upstream pressure variations. *Journal of Geophysical Research*, *94*(a3), 2505–2519. https://doi.org/10.1029/JA094iA03p02505

Spence, H. E., Reeves, G. D., Baker, D. N., Blake, J. B., Bolton, M., Bourdarie, S., et al. (2013). Science goals and overview of the Energetic Particle, Composition, and Thermal Plasma (ECT) suite on NASA's Radiation Belt Storm Probes (RBSP) mission. *Space Science Reviews*, *179*(1-4), 311–336. https://doi.org/10.1007/s11214-013-0007-5

Thorne, R. M., Li, W., Ni, B., Ma, Q., Bortnik, J., Baker, D. N., et al. (2013). Evolution and slow decay of an unusual narrow ring of relativistic electrons near L ~ 3.2 following the September 2012 magnetic storm. *Geophysical Research Letters*, *40*, 3507–3511. https://doi.org/10.1002/grl.50627

Tu, W., Cunningham, G. S., Chen, Y., Henderson, M. G., Camporeale, E., & Reeves, G. D. (2013). Modeling radiation belt electron dynamics during GEM challenge intervals with the DREAM3D diffusion model. *Journal of Geophysical Research: Space Physics*, *118*, 6197–6211. https://doi.org/10.1002/jgra.50560

Waters, C. L., Menk, F. W., & Fraser, B. J. (1991). The resonance structure of low latitude Pc3 geomagnetic pulsations. *Geophysical Research Letters*, *18*(12), 2293–2296. https://doi.org/10.1029/91GL02550

Watt, C. E. J., Rae, I. J., Murphy, K. R., Anekallu, C., Bentley, S., & Forsyth, C. (2017). The parameterization of wave-particle interactions in the Outer Radiation Belt. *Journal of Geophysical Research: Space Physics*, *122*, 9545–9551. https://doi.org/10.1002/2017JA024339

Yau, A. W., Peterson, W. K., & Shelley, E. G. (1988). In T. E. Moore, et al. (Eds.), *Quantitative parametrization of energetic ionospheric ion outflow, in Modeling Magnetospheric Plasma*, *Geophysical Monograph Series* (Vol. 44, pp. 211–217). Washington DC: American Geophysical Union.

References From the Supporting Information

Berube, D., Moldwin, M. B., & Weygand, J. M. (2003). An automated method for the detection of field line resonance frequencies using ground magnetometer techniques. *Journal of Geophysical Research*, *108*(A9), 1348. https://doi.org/10.1029/2002JA009737

Press, W. (1992). *Numerical recipes in C: The art of scientific computing, no. bk. 4 in numerical recipes in C: the art of scientific computing*. New York: William H. Press, Cambridge University Press.

Shue, J.-H., Song, P., Russell, C. T., Steinberg, J. T., Chao, J. K., Zastenker, G., et al. (1998). Magnetopause location under extreme solar wind conditions. *Journal of Geophysical Research*, *103*(A8), 17,691–17,700. https://doi.org/10.1029/98JA01103

Waters, C. L., Samson, J. C., & Donovan, E. F. (1995). The temporal variation of the frequency of high latitude field line resonances. *Journal of Geophysical Research*, *100*(A5), 7987–7996. https://doi.org/10.1029/94JA02712